AGGREGATE Open Access WILEY

Self-assembly of Colloidal Nanoparticles into Encapsulated Hollow Superstructures

Chaolumen Wu, Zhiwei Li, Yaocai Bai, Dung To, Nosang V. Myung, Yadong Yin*

C. Wu, Dr. Z. Li, Dr. Y. Bai, Prof. Y. Yin
Department of Chemistry, University of California, Riverside, CA 92521, USA
E-mail: yadong.yin@ucr.edu

D. To, Pro. N. Myung
Department of Chemical and Biomolecular Engineering, University of Notre Dame, Notre Dame, IN 46556, USA

Keywords: hollow superstructures, nanoparticles, space-confined assembly, emulsion

As a distinct type of nanocapsules, hollow superstructures of inorganic nanoparticles have attracted increasing attention due to their controllable permeability, convenient functionalization, and efficient surface utilization. Conventionally, they are produced by assembling nanoparticles against expensive sacrificial templates. Herein, a general emulsion-based method is reported to assemble colloidal nanoparticles into submicron hollow superstructures, involving first co-assembly of colloidal nanoparticles with organic additives to form clusters, then overcoating the clusters with a polymer shell, and finally removing the organic additives and re-dispersing nanoparticles by exposing to a good solvent. The key to the success of this process is the re-assembly of nanoparticles against the polymer shells as driven by the capillary force during solvent evaporation, producing hollow superstructures. Such a space-confined assembly process can be well controlled by the choice of solvents and their evaporation rates. This general technique provides an open and low-cost platform for creating hollow superstructures of various inorganic nanoparticles, offering many opportunities for exploring unique applications that can take advantage of the collective properties of the constituent nanoparticles and the permeable nanoshell structures.

1. Introduction

Hollow nanoparticles are attracting due to their large surface area and lower material density compared with the solid nanoparticles of similar size, providing opportunities for the

development of materials with new functionalities and improved performance.[1] Template-based synthesis is the most common approach for hollow nanoparticles. Recently, Lin et al developed a soft-template method for the synthesis of hollow nanoparticles by using amphiphilic star-like triblock copolymers as nanoreactors. The intermediate blocks of the copolymers can encapsulate the precursor ions and followed by reduction to yield hollow nanoparticles.[1-2] Hollow superstructures are another type of hollow nanoparticles, composed of densely packed colloidal nanoparticle shells, have promising applications in drug delivery,[3] catalysis,[4] and electrochemical energy storage,[5] as they offer unique opportunities for compartmentalization of active species and controlling their intake and release. Considerable effort has been devoted to assembling colloidal nanoparticles into hollow superstructures primarily by template-based methods. In the hard-template methods, nanoparticles are assembled onto a pre-formed solid template, and subsequent removal of the sacrificial template produces hollow superstructures.[6] The successful assembly requires strong attraction between colloidal nanoparticles and template surface, making it challenging to form robust shells with desirable composition. The high cost involved in synthesizing and removing the hard templates also prevents using these methods for large-scale production. As more convenient and low-cost alternatives, the soft-template methods assemble nanoparticles at liquid-liquid interfaces, typically using emulsion droplets as templates.[7] However, the reduction in Helmholtz free energy of nanoparticles approaches the value of k_BT, resulting in their detachment from the liquid-liquid interface.[8] We recently developed a novel method to overcome this limitation by assembling colloidal nanoparticles at the polymer/water interface within emulsion droplets and subsequently removing the polymer cores by solvent etching.[9] However, this method is only suitable for nanoparticles immiscible with the polymer additives because phase separation is the prerequisite for successful assembly. On the other hand, template-free methods circumvent the usage of templates and directly assemble nanoparticles into hollow superstructures through entropy-driven depletion force, electrostatic interaction, and hydrogen bonding.[10] Although

straightforward, the broad application of the template-free methods is limited to special nanoparticles due to the stringent requirements on the surface capping ligands.

Here, we report a general strategy for the fabrication of submicron hollow superstructures by co-assembling colloidal nanoparticles with miscible organic additives in emulsion droplets (**Scheme 1**). The formation of hollow superstructures is driven by re-dispersing the nanoparticles using a good solvent and re-assembling them through capillary action against a crosslinked polymer capsule. Eliminating the dependence on phase separation may significantly increase the versatility of this soft-template process in producing hollow superstructures from various nanoscale building blocks.

2. Result and discussion

We first choose oleic acid (OA)-capped γ-Fe_2O_3 nanoparticles as model building blocks. These nanoparticles can be conveniently synthesized using a well-reported high-temperature thermolysis reaction, typically exhibiting an average size of 12 nm with narrow size distribution and superparamagnetic property (Figure S1).[9] In a standard assembly process, OA-capped γ-Fe_2O_3 nanoparticles were first washed with a mixed solvent of cyclohexane and acetone, then dispersed in cyclohexane, and finally mixed with sodium dodecyl sulfate (SDS) aqueous solution to form an oil-in-water (O/W) emulsion system. Upon evaporation of cyclohexane, the nanoparticles were assembled into clusters with an average size of 130 nm (Figures 1a, S2), which could be well dispersed in an aqueous solution and further stabilized by coating with a layer of resorcinol formaldehyde (RF), as shown in Figure 1b.[11] Then tetrahydrofuran (THF) was introduced as a good solvent to re-disperse the γ-Fe_2O_3 nanoparticles inside the RF shell (Figure S2c). Finally, the evaporation of THF at 80 ℃ drove the outward diffusion of nanoparticles and their assembly around the inner surface of RF shells, producing hollow superstructures (Figure 1c).

The creation of hollow space within the nanoparticle assemblies results from the loss of capping ligands by dissolution in the good solvent. In the specific case of γ-Fe_2O_3 nanoparticles, the

capping ligand OA can polymerize at the thermolytic temperature (295 °C) via its double bonds to produce oligomers that bind to OA-capped nanoparticles with considerable affinity.[12] These oligomers and excessive OA molecules serve as the organic additives to produce the clusters by co-assembling with γ-Fe_2O_3 nanoparticles. Removing OA and OA oligomers by the good solvent THF produces free space inside the RF shell for the redispersion and assembly of nanoparticles into hollow superstructures. The existence and amount of OA and its oligomers were studied by Matrix-Assisted Laser Desorption/Ionization-Time of Flight (MALDI-TOF) mass spectroscopy and Thermogravimetric Analysis (TGA). As shown in Figure 2(a), the supernatant of the clusters after dispersing in THF was analyzed by MALDI-TOF, showing a peak at 284.34 m/z corresponding to OA and another at 550.66 m/z from OA oligomers (Figure S3).[13] The peaks at 379.12 m/z and 441.05 m/z were related to the matrix solvents. The amount of the OA and OA oligomers of the clusters was quantified by TGA. As shown in Figure 2(d) (red line), the weight loss of ~10 wt% in the temperature range of 150-250 ℃ was mainly contributed by the evaporation of OA. The additional weight loss of ~15 wt% could be attributed to the loss of OA oligomers, occurring in the temperature range of 250-450 ℃.[14] The above results confirm that OA oligomers are produced during the synthesis of γ-Fe_2O_3 nanoparticles, and a large amount (around 25 wt%) of OA and OA oligomers remain in the assembled structures, whose loss by solvent etching results in the generation of the free space within the RF shells.

Figure 2(b) shows the MALDI-TOF of the supernatant after dispersing cluster@RF in THF for 2 h. Interestingly, no peak corresponding to OA or OA oligomers can be found. In contrast, after evaporating THF from the dispersion and then re-dispersing the dried cluster@RF in THF, the MALDI-TOF analysis shows the presence of the OA and OA oligomers in the supernatant, as shown in Figure 2(c). These results indicate that OA and OA oligomers may only diffuse out of the RF shells during the drying process, most likely driven by the capillary action. To further verify the free space formation caused by the loss of OA and OA oligomers, γ-Fe_2O_3

nanoparticles were washed two additional times using cyclohexane/acetone mixed solvent, reducing the organic substances to 10 wt% (Figure 2d). The assembly of such nanoparticles using the above process led to only near-close-packed clusters (Figure 1d). All the above results support that the loss of OA and OA oligomers during the THF evaporation provides free space for the re-assembly of the nanoparticles into hollow superstructures within RF shells.

The amount of OA/oligomers can be used to control the shell thickness of the nanoparticle superstructures since it directly determines the free space inside the RF shells. During the synthesis of γ-Fe_2O_3 nanoparticles, $Fe(CO)_5$ was first decomposed at 295 °C in N_2 atmosphere to produce amorphous $Fe_{1-x}C_x$ nanoparticles (x is the atomic ratio of carbon),[15] which were then oxidized by bubbling air at 200 °C to generate γ-Fe_2O_3 nanoparticles.[9] To further study how the OA/oligomers control the shell thickness, we first washed the $Fe_{1-x}C_x$ nanoparticles 3 times to remove most free OA/oligomers, then dispersed them in ODE with additional OA (2 or 5 mL), followed by oxidation by air bubbling at 200 °C to produce γ-Fe_2O_3 nanoparticles. As shown in Figure 3a, the weight loss of organic substances for the as-synthesized $Fe_{1-x}C_x$ (washed 3 times) and γ-Fe_2O_3 nanoparticles with 2- and 5-mL OA addition (washed once) was about 12 wt%, 22 wt%, and 30 wt%, respectively. As shown in Figure 3b-d, the $Fe_{1-x}C_x$ nanoparticles were assembled into near-close-packed clusters due to the lack of sufficient OA/oligomers. For γ-Fe_2O_3 nanoparticles oxidized with 2 mL OA addition, multi-layer shells were formed, while monolayer-like shells were obtained with 5 mL OA addition. Therefore, the thickness of the nanoparticle shells could be controlled by the ratio of γ-Fe_2O_3 nanoparticles and OA/oligomers, with more OA/oligomers leading to thinner shells. With the further increase of OA/oligomers, nanoparticles are assembled into close-packed nanoparticle shells but with some voids (Figure S4) since there are not enough nanoparticles to fully cover the inner surface of the RF shell and also nanoparticles tend to assemble into close-packed monolayer structures to reduce the surface energy during solvent evaporation.

In our previous method, assembling nanoparticles at the polymer/water interface produces hollow superstructures through the phase separation of nanoparticles and organic additives during solvent evaporation.[9] In the current process, even when the nanoparticles and OA/oligomers are miscible, the RF shell still provides a templating effect for assembling nanoparticles on its inner surface to produce hollow superstructures. As shown in Figure 4, hollow superstructures could be observed when various hydrophobic organic additives such as poly(1-decene), ODE, and hydrogenated poly(1-decene) were used. For poly(1-decene), the core-shell structures were first formed due to the phase separation between poly(1-decene) and nanoparticles (shown in Figure 4a). After the cluster@RF was dispersed in THF, poly(1-decene) was removed from the RF shells during THF evaporation, assembling γ-Fe_2O_3 nanoparticles into hollow superstructures (Figure 4d). The γ-Fe_2O_3 nanoparticles could be homogeneously dispersed in ODE, indicating no phase separation (Figure 4b). When ODE was removed upon THF evaporation, the hollow superstructures can still form (Figure 4e). For hydrogenated poly(1-decene), its initial phase separation from γ-Fe_2O_3 nanoparticles did not occur fully (Figure 4c). However, hollow superstructures can still form after THF evaporation. Therefore, it is reasonable to conclude that the role of organic additives here is mainly to provide free spaces for the assembly of nanoparticles inside the RF shells. Since the capillary-driven assembly is a general process, it only requires the pre-assembly of nanoparticle/organic additives in the emulsion droplets and the subsequent removal of the organic additives by a good solvent through the polymer shells.

Redispersion of nanoparticles inside the RF shells is a key factor to their successful assembly into hollow superstructures. Accordingly, the solvent greatly influences the final assembled structures as it determines the dispersibility of nanoparticles and the solubility of the organic additives. As shown in Figure 5, dimethylformamide (DMF), ethanol, acetone, and THF were chosen to re-assemble the nanoparticles inside the RF shells since all these solvents can dissolve OA/oligomers well. However, the γ-Fe_2O_3 nanoparticles were assembled into hollow

superstructures only in THF. For other solvents, γ-Fe_2O_3 nanoparticles tend to aggregate and assemble into irregular hollow structures. The polarity difference between these four solvents results in the different dispersion behaviors of nanoparticles. With a relatively low polarity of 0.207, THF is a good solvent for dispersing hydrophobic γ-Fe_2O_3 nanoparticles. In contrast, the polarity of DMF, ethanol, and acetone is 0.386, 0.654, and 0.355, respectively. They cannot fully disperse γ-Fe_2O_3 nanoparticles, as shown in the size distribution plots in Figure 5. The assembly process of nanoparticles within different solvents is schematically illustrated in Figure 5e. Nanoparticles can move freely in good solvents and re-assemble into well-defined hollow superstructures, while they remain aggregated upon exposure to poor solvents and therefore assemble into irregular structures.

The re-assembly of nanoparticles at the inner surface of the RF shells can also be controlled by the evaporation temperature. When evaporation was performed at a low temperature (20 °C), the assembly of nanoparticles appeared to be more random, resulting in irregular hollow structures (Figure 6a). In contrast, increasing the evaporation temperature has consistently improved the regularity of the assembled nanoparticle shells, as shown in Figures 6b and 6c. We believe two factors may contribute to the temperature-dependent assembly behavior, including the enhanced colloidal dispersity of the nanoparticles and their improved outward diffusion rate at higher temperatures. The rate of nanoparticle diffusion depends strongly on solvent evaporation rate, which increases with increasing temperature and decreasing ambient pressure. This understanding was further proved by carrying out the assembly at 20 °C, but with a reduced pressure of 0.068 MPa. As shown in Figure 6d, the faster solvent evaporation led to more regular hollow superstructures.

After re-assembling nanoparticles into hollow superstructures, the RF shell can be converted into carbon by calcination while retaining the magnetic property and morphology of the hollow superstructures. Controlling the extent of calcination also allows fine-tuning the shell thickness. As shown in Figure 7a-c, the original shell thickness of 27 nm was reduced to 13 nm and 8 nm

by 2-h calcination in air at 250 °C and 300 °C, respectively. The TGA curves in Figure 7e also show weight loss of 26 wt% and 35 wt% after calcination at 250 °C and 300 °C due to the combustion of organic substances. The RF shell was removed entirely when the calcination temperature was further increased to 350 °C (Figure 7d), corresponding to a significant weight loss of 57 wt%. The above four samples were further characterized by FTIR to study the chemical change of the shells upon calcination at different temperatures. As shown in Figure 7f, the typical RF peaks (e.g., 3200 cm^{-1} for -OH groups) disappeared after the calcination at 250 and 300 °C, and the peak around 1630 cm^{-1} corresponding to aromatic groups like carbonyl gradually diminished.[16] All the RF peaks disappeared after the calcination at 350 °C, further confirming the complete removal of the RF shells. Interestingly, the hollow superstructures were well maintained during the calcination, even after the complete removal of the shells. The partial interparticle fusion contributes to formation of the stable hollow superstructures (as shown in Figure S5), and the coalescence between the neighboring nanoparticles is further confirmed by the increased intensity of XRD peaks in Figure 7h (red curve). The magnetic property was maintained even after calcination at 350 °C, and the assembled structures can be completely separated within one min using a rare earth magnet (as shown in Figure S6a). As shown in the magnetization curves in Figure 7g, all the samples were superparamagnetic. The saturation magnetization values were increased from 23 to 38 and 50 emu g^{-1} for samples calcined at 250, 300, and 350 °C due to the increasing mass ratio of magnetic particles in the samples. The original γ-Fe_2O_3 nanoparticles have a higher saturation magnetization value (55 emu g^{-1}) than the sample calcinated at 350 °C, indicating partial oxidation of maghemite to hematite during calcination confirmed by the XRD analysis in Figure 7h. The sample calcined at 350 °C showed primary peaks corresponding to maghemite γ-Fe_2O_3 (JCPDS Card No. 39-1346), similar to the original nanoparticles except for a small peak corresponding to the hematite phase (JCPDS Card No.33-0664).[9]

The polymer shells can be fully converted into carbon by further calcination at 500 ℃ in N_2 atmosphere.[16] We chose the above 300 ℃ calcinated sample as an example to show the conversion, and the carbonized sample could also maintain the hollow morphology (shown in the TEM image of Figure S6c) and magnetic property (Figure S6b), displaying characteristic peaks of γ-Fe_2O_3 in the XRD pattern (Figure 7h). The slight increase in grain size of the calcined samples, as indicated by the increased intensity of XRD peaks, suggests a possible interparticle fusion, which contributes to the formation of stable hollow superstructures. Thus, the polymer shells not only serve as templates for the assembly of nanoparticles into hollow superstructures but also help maintain the morphology of the hollow superstructures during calcination. The conversion of the shell into carbon may also provide opportunities for broader applications.

The current assembly strategy is general and can assemble various hydrophobic colloidal nanoparticles with different compositions, sizes, and shapes into hollow superstructures. Figure 8 shows a few examples of hollow superstructures assembled from OA-capped CdSe,[17] TOPO-capped ZrO_2,[18] OA-capped $CoFe_2O_4$,[19] and TOPO-capped Cu_2S nanoplate.[20] The size distributions of these nanoparticles are shown in Figure S7. It is worth noting that the hollow superstructures assembled from the CdSe quantum dots still displayed good photoluminescence properties, as shown in the inset of Figure 8e.

3. Conclusion

In summary, here we present a general strategy for the fabrication of submicron hollow superstructures by assembling hydrophobic colloidal nanoparticles within emulsion droplets and then re-assembling them against polymer shells through solvent dissolution and evaporation. Unlike previous emulsion-based method that relies on phase separation of nanoparticles and organic additives, the current strategy has no requirement on the miscibility of nanoparticles and organic additives. Instead, organic additives only serve as a sacrificial agent to create spaces for re-assembling nanoparticles into hollow superstructures. Eliminating

the dependence on phase separation may significantly increase the versatility of this soft-template process in producing hollow superstructures from various nanoscale building blocks. The key to the success of this strategy is the encapsulation of nanoparticle/organic additive clusters in a crosslinked polymer shell, which further serves as a template to guide the re-assembly of nanoparticles on its inner surface into well-defined hollow superstructures. The re-assembly of nanoparticles is ensured using a good solvent, which removes the organic additives and induces outward diffusion of nanoparticles toward the polymer shell. By controlling the nanoparticle/additive ratio in the emulsion droplets, the thickness of hollow superstructures can be fine-tuned. Also, the effects of organic additives, solvents, and solvent evaporation rate were systematically studied to reveal the working principle of this assembly strategy. Furthermore, the polymer shells can be converted into carbon with fine tunability of the thickness by calcination, maintaining the original hollow morphology of the nanoparticle assemblies and their magnetic properties. The current work not only provides a general strategy for assembling colloidal nanoparticles into hollow superstructures but also demonstrates exciting opportunities that may be offered by assembling colloidal nanoparticles within nanoscale confinements.

Experimental Section

Synthesis of γ-Fe_2O_3 nanoparticles

Superparamagnetic γ-Fe_2O_3 nanoparticles were synthesized using a thermolysis process.[9] $Fe(CO)_5$ (0.4 mL, 3.04 mmol) was added to a mixture containing 20 mL of 1-octadecene and 1.5 mL of oleic acid at 100 °C under N_2. The solution was then heated to 295 °C under the N_2 atmosphere and maintained at this temperature for 1 h. After cooling down to 200 °C, the solution was bubbled with air for 2 h. After cooling down to room temperature, a mixture of cyclohexane/acetone was added to the solution to precipitate γ-Fe_2O_3 nanoparticles, which were

then separated by centrifugation. Finally, the resulting black powder was re-dispersed in 8 mL cyclohexane.

Controlling the amount of OA and OA oligomers of γ-Fe_2O_3 nanoparticles

The amount of OA and OA oligomers of γ-Fe_2O_3 nanoparticles can be controlled during the oxidation process of the synthesis. After the reaction at 295 °C under N_2 atmosphere for 1 h, the solution was cooled down to room temperature and washed three times with cyclohexane/acetone mixture solvent to completely remove the extra OA/OA oligomers. The resulting nanoparticles were dispersed in 20 mL ODE containing different amounts of OA (2 mL and 5 mL). The solution was heated to 200 °C and kept at this temperature for 2 h with bubbling air. The solution was cooled down to room temperature and washed with cyclohexane/acetone mixed solvent once to get the γ-Fe_2O_3 nanoparticles with different amounts of OA and OA oligomers.

Synthesis of ZrO_2 nanoparticles

ZrO_2 nanoparticles were prepared by a nonhydrolytic solution-based reaction.[18] TOPO (10 g) was heated at 150 °C for 30 minutes under vacuum. After cooling the solution temperature to 60 °C under N_2 atmosphere, zirconium (IV) isopropoxide propanol complex (1.56 g) and $ZrCl_4$ (1.16 g) were added into the solution. The resulting mixture was then heated to 340 °C and further heated for 2 hours at 340 °C to ensure a complete reaction. After cooling the system down to 80 °C, 20 mL of acetone was added to yield a white precipitate, which was isolated by centrifugation and subsequently washed with a cyclohexane/acetone mixture to remove extra surfactant. The resulting powder was re-dispersed in 8 mL cyclohexane.

Synthesis of CdSe nanoparticles

CdSe QDs were synthesized by the hot injection method from the literature.[17] Typically, CdO (256 mg) was added into oleic acid (1.9 mL) and ODE (40 mL) in a 100 mL three-neck flask and heated to 200 °C under an N_2 flow to obtain a precursor solution. This solution was cooled down to 160 °C, after which ODA (3.0 g) was added and heated up to 240 °C under an N_2 flow.

A selenium solution (780 mg of Se dissolved in 5 mL TOP and 5 mL ODE) was injected into the above solution, and the reaction continued for 4 min before quickly cooling to room temperature. Subsequently, the as-prepared CdSe QDs were washed with cyclohexane and ethanol once and finally dispersed in 8 mL cyclohexane.

Synthesis of $CoFe_2O_4$ nanoparticles

The spherical $CoFe_2O_4$ nanocrystals were synthesized using a nonhydrolytic reaction.[19] In a typical synthesis, 2 mmol of $Co(acac)_2$, 40 mL of phenyl ether, 20 mmol of 1,2-hexadecanediol, 10 mL of oleic acid, and 10 mL of oleylamine were mixed and heated to 140°C followed by a droplet addition of 4 mmol $Fe(acac)_3$ in 20 mL of a phenyl ether solution. The temperature was then increased quickly to 260 °C, and the mixture was kept at reflux for 30 min before being cooled down to room temperature. After adding ethanol and centrifuging, spherical $CoFe_2O_4$ nanocrystals with a diameter of 5 nm were obtained.

Synthesis of Cu_2S nanodisks

The Cu_2S nanodisks were synthesized by the method reported in our previous paper.[20] Cuprous acetate (0.0488 g), TOPO (1 g), and 1-octadecene (30 mL) were mixed in a three-neck flask and then degassed under N_2 flow for 30 min. Upon heating the solution to 160 ℃, 1 mL of 1-dodecanethiol was injected quickly into the flask under vigorous stirring. The resulting mixture was further heated to 200 ℃ then reacted for 4 h. The product was collected by adding an excess amount of methanol. The final Cu_2S nanoparticles were dispersed in 8 mL cyclohexane.

Self-assembly of nanoparticles and organic additives into clusters

The nanoparticle/organic additive clusters were assembled in emulsion oil droplets by evaporating the low-boiling-point solvent (the oil phase). In a typical experiment, 1 mL of a cyclohexane solution of nanoparticles with a certain amount of organic additives was added into an aqueous solution of SDS (56 mg in 10 mL of H_2O), followed by sonication for 5 min. The mixture was then heated to 65 °C in a water bath for 4 h. After that, the reaction solution

was cooled down to room temperature. The final products were washed with water one time and re-dispersed in 3 mL of water.

RF coating on clusters and re-assembly of nanoparticles in RF shells

Nanoparticles/organic additive clusters were coated with a layer of RF by using a method developed by our group.[11] Typically, the clusters were dispersed in 28 mL of an aqueous solution containing 12.5 mg R, 17.5 uL F, and 100 uL ammonia (2.8wt%). The above solution was sonicated for 1 h, transferred into 100 mL three-neck flask, and refluxed at 100 °C for 1 h. The final products were washed with water once and did magnetic separation to get the cluster@RF. Then, the cluster@RF was dispersed in THF to dissolve the oil phase and disperse the nanoparticles in the RF shell. The nanoparticles can re-assemble into hollow superstructures in the RF shell by evaporating the solvent (THF) at 80 °C.

Supporting Information

Supporting Information is available from the Wiley Online Library or from the author.

Acknowledgements

This work was supported by the U.S. National Science Foundation (DMR-1810485). The authors declare no conflict of interest.

Received: ((will be filled in by the editorial staff))
Revised: ((will be filled in by the editorial staff))
Published online: ((will be filled in by the editorial staff))

References

[1] X. Pang, L. Zhao, W. Han, X. Xin, Z. Lin, *Nat Nanotechnol* **2013**, *8*, 426.
[2] a) Y. Chen, D. Yang, Y. J. Yoon, X. Pang, Z. Wang, J. Jung, Y. He, Y. W. Harn, M. He, S. Zhang, *J. Am. Chem. Soc.* **2017**, *139*, 12956; b) S. Pan, Y. Chen, Z. Wang, Y.-W. Harn, J. Yu, A. Wang, M. J. Smith, Z. Li, V. V. Tsukruk, J. Peng, *Nano Energy* **2020**, *77*, 105043.
[3] J. Song, X. Yang, Z. Yang, L. Lin, Y. Liu, Z. Zhou, Z. Shen, G. Yu, Y. Dai, O. Jacobson, *ACS nano* **2017**, *11*, 6102.
[4] D. V. Shinde, L. D. Trizio, Z. Dang, M. Prato, R. Gaspari, L. Manna, *Chem. Mater.* **2017**, *29*, 7032.
[5] H. You, L. Zhang, Y. Jiang, T. Shao, M. Li, J. Gong, *J. Mater. Chem. A* **2018**, *6*, 5265.
[6] F. Caruso, R. A. Caruso, H. Möhwald, *Science* **1998**, *282*, 1111.
[7] Y. Lin, H. Skaff, T. Emrick, A. Dinsmore, T. P. Russell, *Science* **2003**, *299*, 226.

[8] T. Bollhorst, K. Rezwan, M. Maas, *Chem. Soc. Rev* **2017**, *46*, 2091.
[9] C. Wu, Z. Lu, Z. Li, Y. Yin, *Small Structures* **2021**, *2*, 2100005.
[10] J. S. Haataja, J. V. Timonen, S. Malola, P. Engelhardt, N. Houbenov, M. Lahtinen, H. Häkkinen, O. Ikkala, *Angew. Chem.* **2017**, *129*, 6573.
[11] a) Z. Li, J. Jin, F. Yang, N. Song, Y. Yin, *Nat Commun* **2020**, *11*, 1; b) Z. Li, Q. Fan, C. Wu, Y. Li, C. Cheng, Y. Yin, *Nano Lett* **2020**, *20*, 8242.
[12] T. Hu, Q. Ji, W. H. Chong, W. Xin, X. Liu, H. Chen, *Nanoscale* **2020**, *12*, 18640.
[13] H.-M. Hung, Y. Katrib, S. T. Martin, *J Phys Chem A* **2005**, *109*, 4517.
[14] N. V. Jadhav, A. I. Prasad, A. Kumar, R. Mishra, S. Dhara, K. Babu, C. Prajapat, N. Misra, R. Ningthoujam, B. Pandey, *Colloids Surf B Biointerfaces* **2013**, *108*, 158.
[15] a) T. Hyeon, S. S. Lee, J. Park, Y. Chung, H. B. Na, *J. Am. Chem. Soc.* **2001**, *123*, 12798; b) J. Van Wonterghem, S. Mørup, S. W. Charles, S. Wells, *J. Colloid Interface Sci.* **1988**, *121*, 558; c) J. van Wonterghem, S. Mørup, S. W. Charles, S. Wells, J. Villadsen, *Phys Rev Lett* **1985**, *55*, 410.
[16] V. G. Pol, L. K. Shrestha, K. Ariga, *ACS Appl. Mater. Interfaces* **2014**, *6*, 10649.
[17] R. Shi, Y. Cao, Y. Bao, Y. Zhao, G. I. Waterhouse, Z. Fang, L. Z. Wu, C. H. Tung, Y. Yin, T. Zhang, *Adv. Mater* **2017**, *29*, 1700803.
[18] J. Joo, H. B. Na, T. Yu, J. H. Yu, Y. W. Kim, F. Wu, J. Z. Zhang, T. Hyeon, *J. Am. Chem. Soc.* **2003**, *125*, 11100.
[19] Q. Song, Z. J. Zhang, *J. Am. Chem. Soc.* **2004**, *126*, 6164.
[20] Y. Wang, Y. Hu, Q. Zhang, J. Ge, Z. Lu, Y. Hou, Y. Yin, *Inorg. Chem.* **2010**, *49*, 6601.

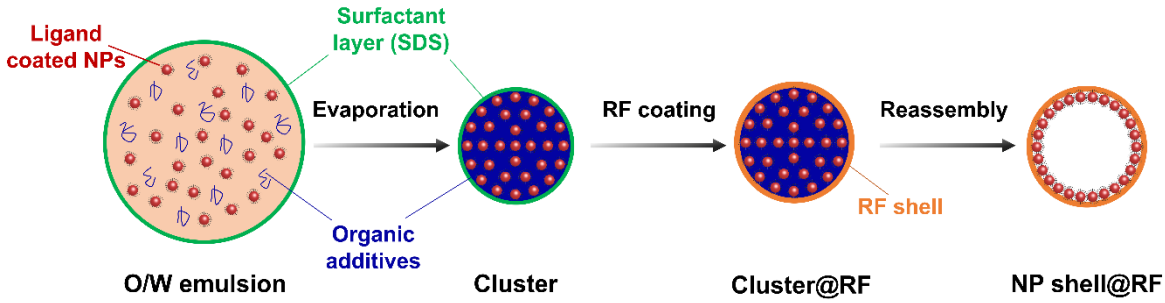

Scheme 1. The process of assembling colloidal nanoparticles into hollow superstructures within polymer nanocapsules.

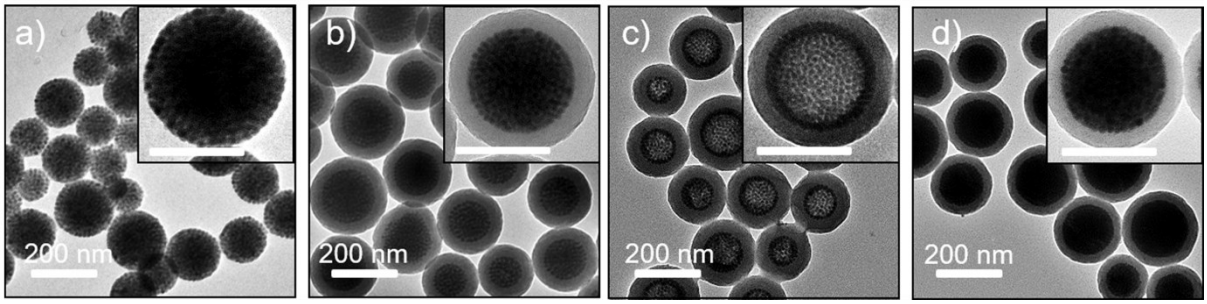

Figure 1. (a, b) TEM images of γ-Fe_2O_3 nanoparticle clusters before (a) and after (b) RF coating. (c, d) TEM images of the re-assembled structures after re-dispersing γ-Fe_2O_3@RF samples in THF and then evaporating the solvent, with the original γ-Fe_2O_3 nanoparticles being washed one (c) and three (d) times using a mixed solvent of cyclohexane and acetone before forming clusters. Insets are high-magnification TEM images with scale bars of 100 nm**.**

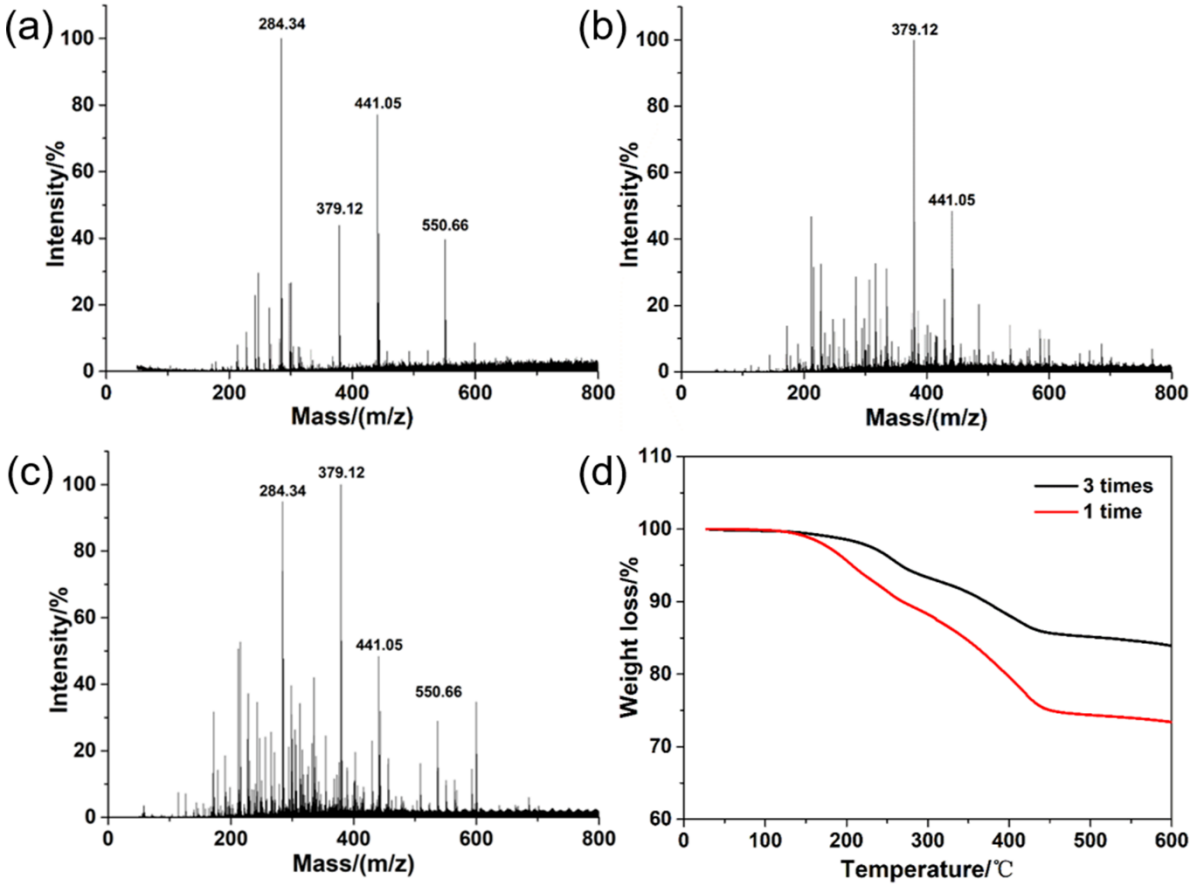

Figure 2. (a-c) MALDI-TOF spectra of supernatant solutions obtained by (a) centrifuging a dispersion of γ-Fe_2O_3 nanoparticle clusters in water, (b) centrifuging a dispersion of γ-Fe_2O_3 cluster@RF in THF, (c) evaporating the solvent from a THF dispersion of γ-Fe_2O_3 cluster@RF, re-dispersing the dried sample in THF, and then centrifuging the resulting dispersion. (d) TGA of the γ-Fe_2O_3 nanoparticle clusters assembled from the nanoparticles pre-washed one and three times.

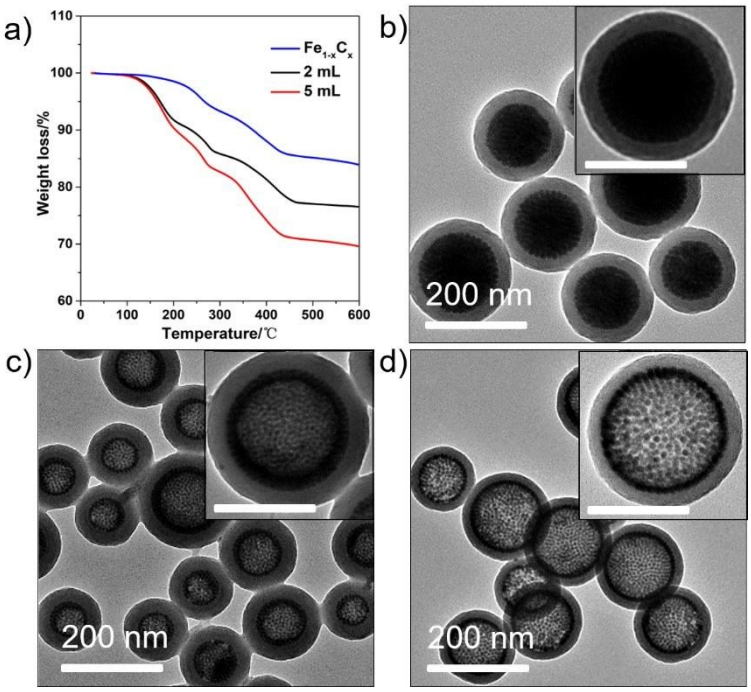

Figure 3. (a) TGA spectra of the amorphous $Fe_{1-x}C_x$ nanoparticles after three-time washing and γ-Fe_2O_3 nanoparticles after one-time washing. The γ-Fe_2O_3 nanoparticles were prepared by bubbling air through the dispersion of $Fe_{1-x}C_x$ nanoparticles at 200 ℃ in the presence of 2 mL and 5 mL OA. (b-d) TEM images of the cluster@RF samples after the standard re-assembly process. The clusters were assembled from $Fe_{1-x}C_x$ nanoparticles (b) and γ-Fe_2O_3 nanoparticles prepared by oxidation in the presence of 2 mL (c) and 5 mL (d) OA. Insets are high-magnification TEM images with scale bars of 100 nm.

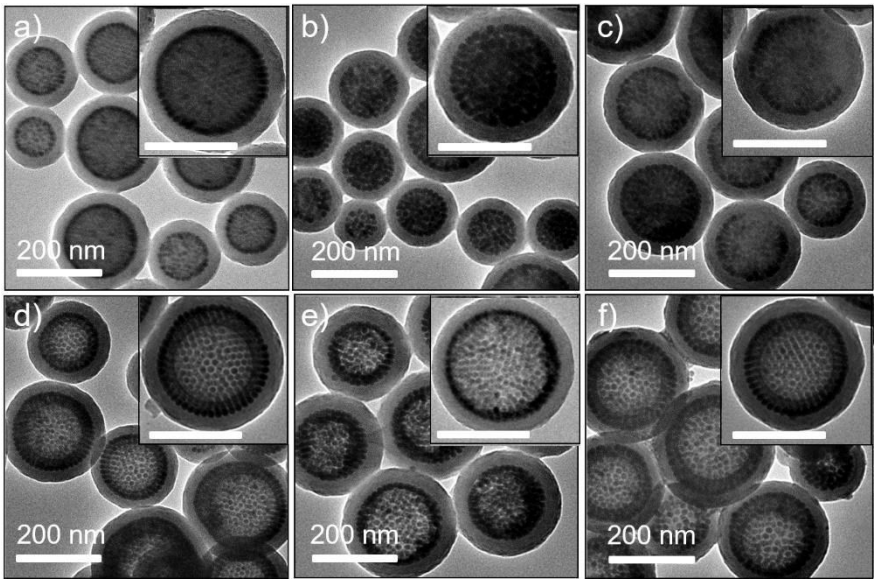

Figure 4. TEM images of various cluster@RF samples before (a-c) and after (d-f) the standard re-assembly process. The clusters were prepared by co-assembling γ-Fe_2O_3 nanoparticles with different organic additives: (a, d) poly(1-decene), (b, e) ODE, and (c, f) hydrogenated poly(1-decene). Insets are high-magnification TEM images with scale bars of 100 nm.

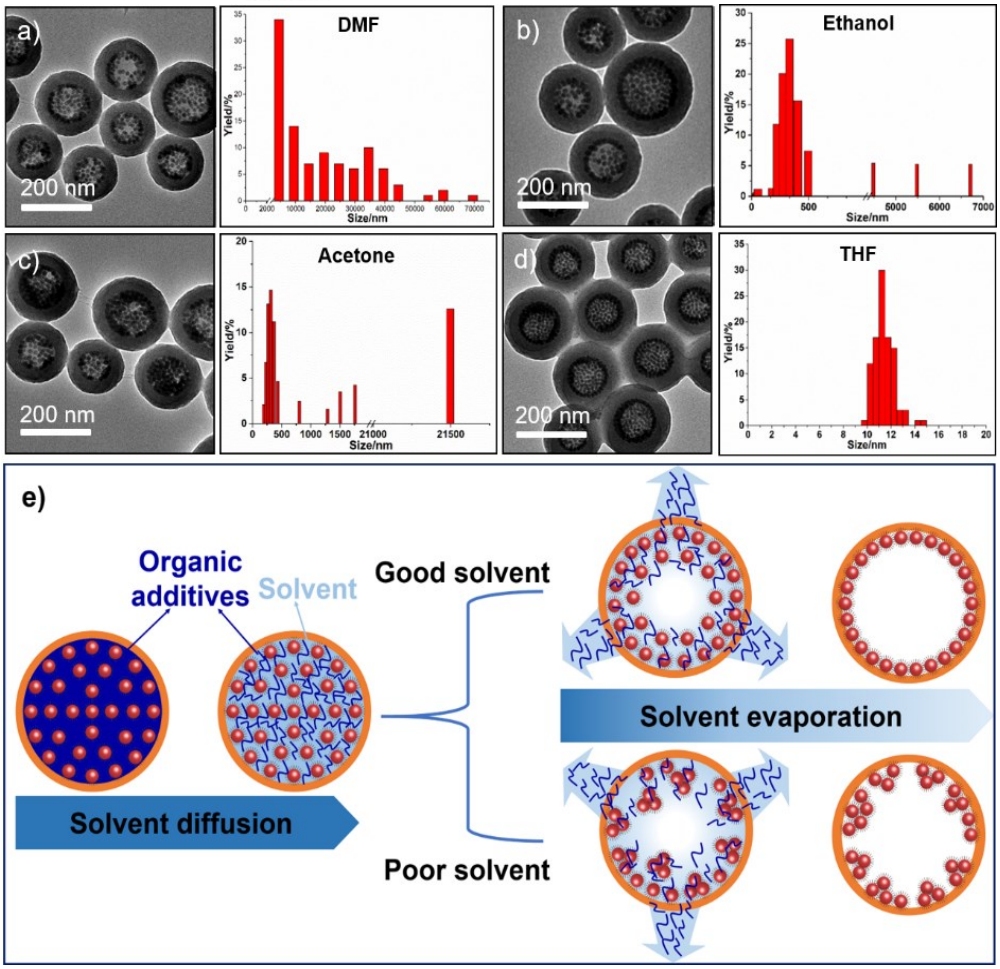

Figure 5. (a-d) TEM images of the cluster@RF samples after the re-assembly using different solvents: (a) DMF, (b) ethanol, (c) acetone, and (d) THF. The histograms are the size distribution of γ-Fe_2O_3 nanoparticles in different solvents. (e) Schematic illustration showing the re-assembly of nanoparticles within the RF shells using good and poor solvents.

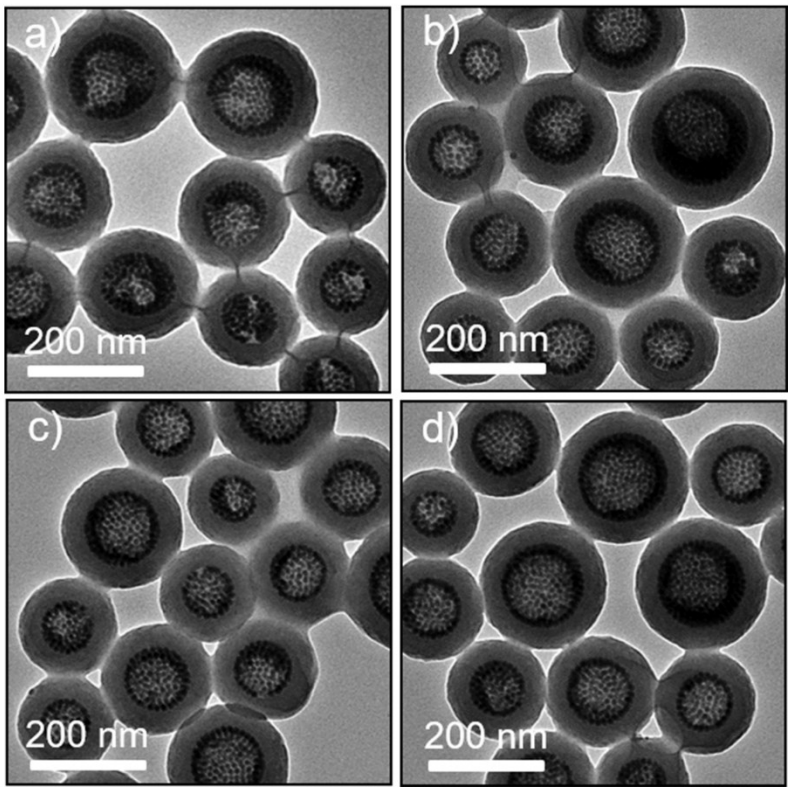

Figure 6. TEM images of nanoparticle@RF samples re-assembled using THF (a-c) under atmospheric pressure at the temperature of 20 ℃ (a), 50 ℃ (b), and 80 ℃(c); and (d) under reduced pressure (0.068 MPa) at 20 ℃.

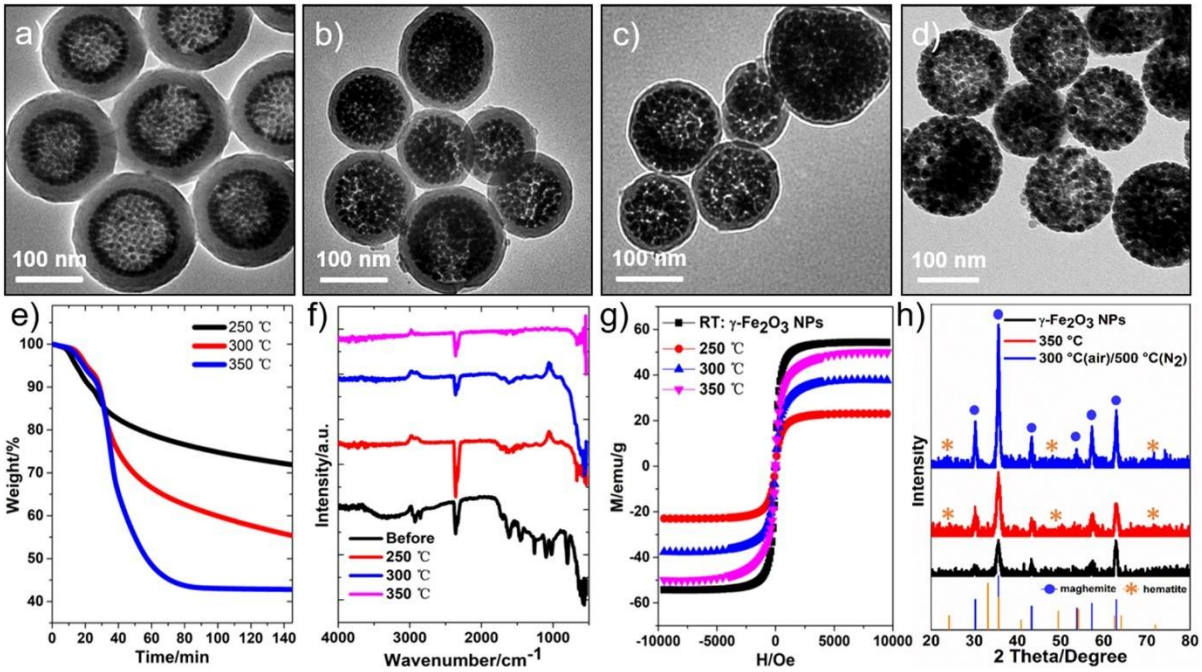

Figure 7. (a-d) TEM images of RF coated γ-Fe_2O_3 hollow superstructures after calcination at different temperatures in air for 2 h: (a) original sample, (b) 250 °C, (c) 300 °C, and (d) 350 °C. (e) TGA of the above three calcined samples. (f) Fourier-transform infrared (FTIR) spectra of the samples before and after calcination at different temperatures. g) Hysteresis loops of the γ-Fe_2O_3 nanoparticles and the RF coated hollow superstructures after calcination in air under different temperatures. (h) X-ray diffraction (XRD) spectra of the γ-Fe_2O_3 nanoparticles, the hollow superstructures after calcination at 350 °C in air for 2h, and the carbonized sample after calcined at 300 °C in air for 2 h and then 500 °C in N_2 for 2 h.

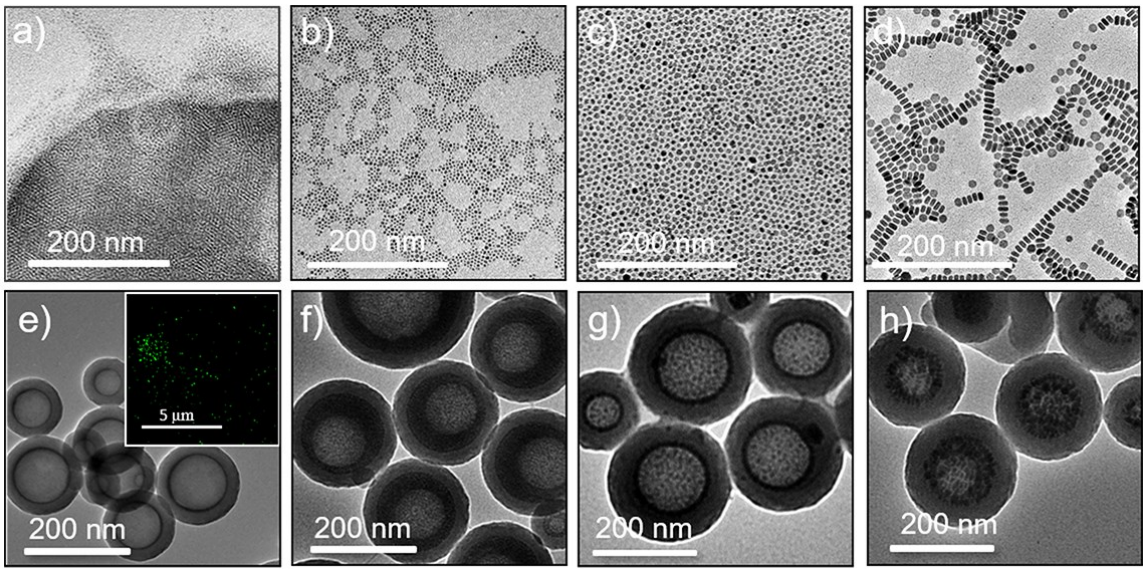

Figure 8. TEM images of nanoparticles of various materials (a-d) and corresponding hollow superstructures assembled in RF shells (e-h): (a, e) CdSe@OA, (b, f) ZrO_2@TOPO, (c, g) $CoFe_2O_4$@OA and (d, h) Cu_2S@TOPO nanoplates. Inset in (e) is the fluorescent microscopy image of CdSe hollow superstructures excited by a 405-nm laser.

A general strategy is developed to fabricate submicron hollow superstructures by assembling nanoparticles against encapsulating polymer shells as driven by the capillary action during solvent evaporation. Such a nanoscale space-confined assembly process can be well controlled by choice of solvents and their evaporation rates.

Keywords: hollow superstructures, nanoparticles, space-confined assembly, emulsion

Chaolumen Wu, Zhiwei Li, Yaocai Bai, Dung To, Nosang V. Myung, Yadong Yin*

Self-assembly of Colloidal Nanoparticles into Encapsulated Hollow Superstructures